

Supporting information for

Facet-dependent adsorption of aluminum(III) on hematite nanocrystals and the
influence on mineral transformation

Wentao Wang^{1,2}, Wenjun Zhang^{1,2}, Yuke Fan^{1,2}, Chenchen Qu^{1,2}, Wenyan Ren^{1,2}, Xiaopeng
Huang³, Mei Hong⁴, Fan Liu^{1,2}, Hui Yin^{1,2,*}

¹Key Laboratory of Arable Land Conservation (Middle and Lower Reaches of Yangtse River),
Ministry of Agriculture and Rural affairs, College of Resources and Environment, Huazhong
Agricultural University, Wuhan 430070, China

²State Environmental Protection Key Laboratory of Soil Health and Green Remediation, Ministry
of Ecology and Environment, Wuhan 430070, China

³Department of Civil and Environmental Engineering, Carnegie Mellon University, Pittsburgh,
Pennsylvania 15213, United States

⁴College of Grassland, Resources and Environment, Inner Mongolia Agricultural University,
Hohhot 010018, China

Corresponding Authors:

Tel.: +86 27 87280271. Fax: +86 27 87288618.

Email: yinhui666@mail.hzau.edu.cn (H. Yin).

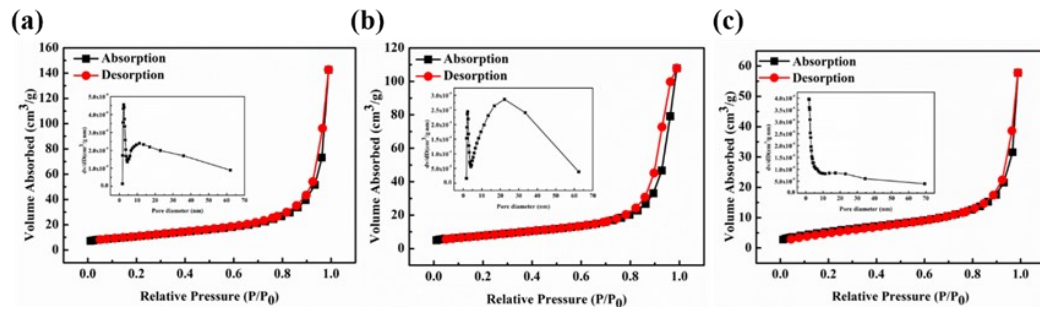


Figure S1. N_2 adsorption-desorption isotherms and pore size distribution of hematite samples with different exposed faces. (a) HNP, (b) HNC, and (c) HNR.

Text S1. Estimation of Relative Abundance of Exposed Crystal Facets.

The geometric models for the hematite nanocrystals were established according to the dominant exposed facets identified using high-resolution transmission electron microscopy (HRTEM), and the averaged size measurements on the transmission electron microscopy (TEM) analysis. The detailed procedures for calculating the relative abundance of the exposed facets were as following:

Hematite nanosheets (HNPs) were composed of two symmetric {001} facets on the basal surfaces and six equivalent {102} facets on the side surfaces (**Fig. S2**). The average side lengths and heights of these hexagonal sheets are 85.5 ± 4.1 nm and 12.2 ± 1.9 nm respectively. The relative abundances of {001} (%S{001}) and {102} (%S{102}) faces were calculated as:

$$\%S\{001\} = \frac{\frac{3}{2}\sqrt{3} \times 85.5^2 \times 2}{\frac{3}{2}\sqrt{3} \times 85.5^2 \times 2 + 12.2 \times 85.5 \times 6} = 86\% \quad (1)$$

$$\%S\{102\} = 1 - \%S\{001\} = 14\% \quad (2)$$

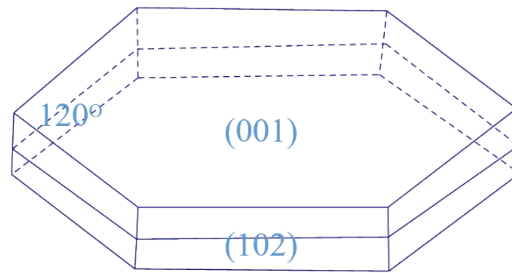


Fig. S2 Geometrical model of HNR

Hematite nanorods (HNRs) were composed of two symmetric {001} facets on the basal surfaces, and two equivalent {110} facets, two equivalent {120} facets, and two equivalent {210} facets on the side surfaces (**Fig. S3**). HNR are regular rods with length, width, and height of 629.4 ± 76.3 nm, 51.0 ± 13.9 nm and 50.2 ± 7.6 nm. The relative abundances of each surface (%S{110}, %S{001} and %S{120}+{210}) were calculated as:

$$\%S\{110\} = \frac{50.2 \times 629.4 \times 2}{(50.2 \times 629.4 \times 2 + 51 \times 629.4 \times 2 + 51 \times 50.2 \times 2)} = 48\% \quad (3)$$

$$\%S\{001\} = \frac{51 \times 629.4 \times 2}{(50.2 \times 629.4 \times 2 + 51 \times 629.4 \times 2 + 51 \times 50.2 \times 2)} = 48\% \quad (4)$$

$$\%S\{120\} + \{210\} = 1 - \%S\{110\} - \%S\{001\} = 4\% \quad (5)$$

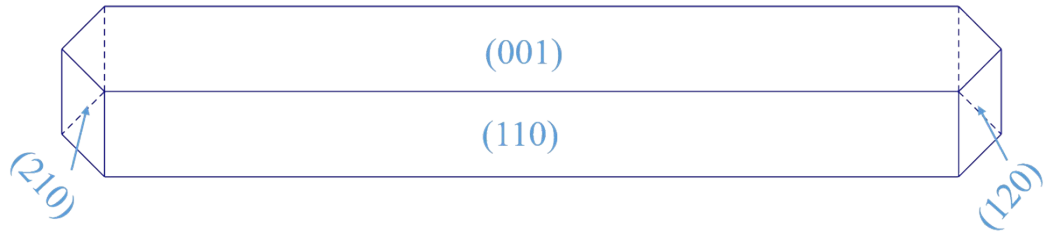


Fig. S3 Geometrical model of HNR

Hematite nanocubes (HNCs) were composed of eight equivalent {012} facets with nearly 100% exposure of the {012} facets of HNCs (**Fig. S4**).

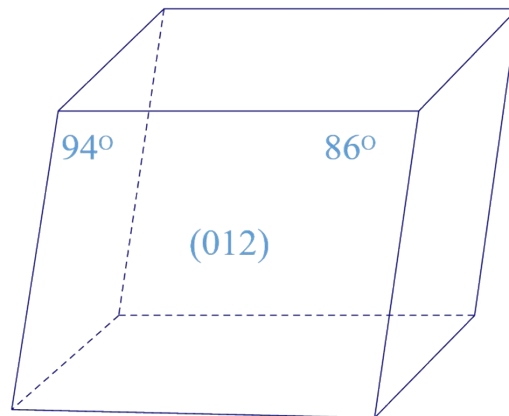


Fig. S4 Geometrical model of HNC

Text S2. Estimation of the Densities of Different Types of Surface Hydroxyl Groups.

The densities of different types of OH groups (i.e., numbers of $-\text{FeOH}$, $-\text{Fe}_2\text{OH}$ and $-\text{Fe}_3\text{OH}$ sites per nm^2) on a given facet were obtained following the method described in literatures¹⁻³ (**Table S1**). And then the densities of these active sites for each hematite were calculated from the specific surface areas, the proportions of different exposed faces, and the densities of each OH group on a given facet⁴ (**Table S1**).

Table S1. Densities of different types of hydroxyl groups on the different facets and total surface hydroxyl species on hematite crystals.

Facet	$-\text{FeOH}$ (sites $\cdot\text{nm}^{-2}$)	$-\text{Fe}_2\text{OH}$ (sites $\cdot\text{nm}^{-2}$)	$-\text{Fe}_3\text{OH}$ (sites $\cdot\text{nm}^{-2}$)
{001}	—	13.7	—
{110}	5.0	5.0	5.0
{012}	5.0	—	5.0
{102}	5.1	5.1	5.9
Sample	Total surface hydroxyl species ($\mu\text{mol}\cdot\text{m}^{-2}$)		
HNP	1.21	21.07	1.43
HNC	8.42	—	8.42
HNR	4.92	26.47	4.42

Text S3 Chemical speciation of Al ions

Aluminum ions can exist as various species⁵⁻⁷. In order to help understand the adsorption behaviors of Al^{3+} on hematite crystals, Al species under different pH conditions were calculated by Visual MINTEQ^{8,9}. Firstly, the relative proportions of dissolved and precipitated Al at low ionic strength ($[\text{NaNO}_3] = 0.01 \text{ M}$) were calculated (**Fig. S5a**). When $\text{pH} \leq 4$ or ≥ 10 , all Al are dissolved. During pH 4-6, the proportion of dissolved Al is gradually decreased to zero and the proportion of Al precipitated is increased to 100 %, while the inverse is true during pH 8-10. For the dissolved Al species (**Fig. S5b**), Al mainly exists as free Al^{3+} when $\text{pH} < 4$. With increasing pH, the proportion of free Al^{3+} is gradually decreased to zero at pH 6. Concurrently, the proportion of $[\text{AlOH}]^{2+}$ starts to increase from pH 4 while those of $[\text{Al}(\text{OH})_2]^+$ and $[\text{Al}(\text{OH})_3]$ start to increase from pH 5. The proportions of these species maximize at pH 5, 5 and 6 and finally disappear at pH 7, 7 and 8, respectively. Anion $[\text{Al}(\text{OH})_4]^-$ appears at pH 6, and becomes the only species in solution at pH 8 till to pH 12.

At high ionic strength ($[\text{NaNO}_3] = 0.72 \text{ M}$), the relative proportions of dissolved and precipitated Al are almost the same as that at low ionic strength, except that the pH range that all Al exists in dissolved form in acid conditions extend to pH 5 (**Fig. S5c**). So is the Al species in the dissolved form (**Fig. S5d**). The proportion of $[\text{Al}_3(\text{OH})_4]^{5+}$ is greatly increased compared to that at low ionic strength. The peak center for $[\text{AlOH}]^{2+}$ moves to pH 6 compared to pH 5 at low ionic strength.

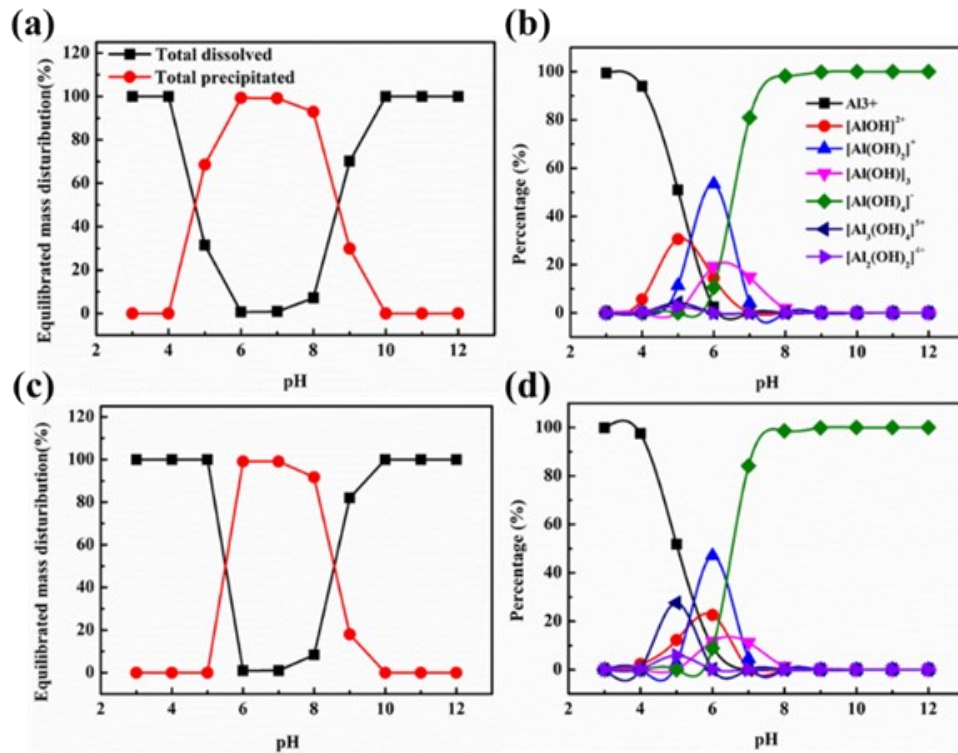


Fig. S5 The changes of (a, c) total Al and (b, d) dissolved Al species with pH for 1 mM Al^{3+} at 25 °C at low ionic strength ($[NaNO_3] = 0.01$ M) and high ionic strength ($[NaNO_3] = 0.72$ M) respectively.

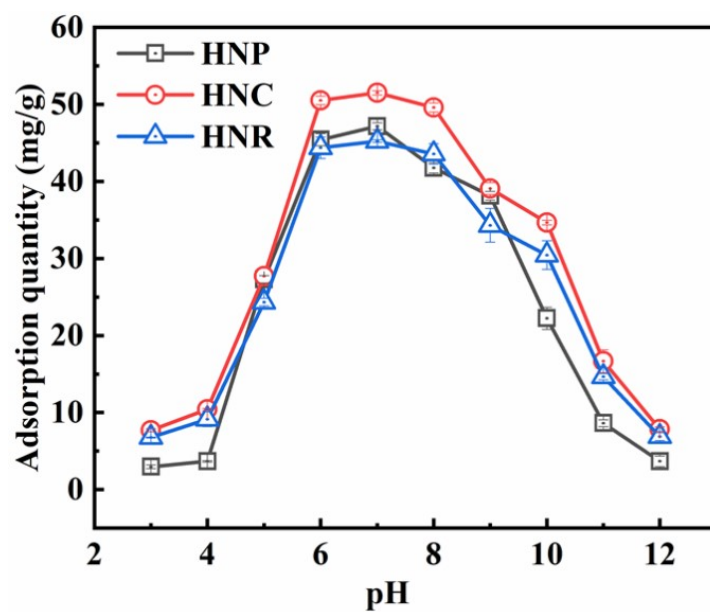


Figure S6. Changes of the adsorption densities of Al ions on three kinds of hematite crystals with pH ranging from 3 to 12. Experimental conditions: [hematite] = 0.5 g·L⁻¹, [Al³⁺] = 1 mM, and [NaNO₃] = 0.01 M.

Table S2 The Langmuir fitting parameters for isothermal adsorption of aluminum on three synthetic hematite samples.

Sample	pH	Xm ($\mu\text{mol}/\text{m}^2$)	K _L	R ²
HNP	4	3.59	0.0491	0.983
	12	4.11	0.0682	0.994
HNC	4	8.52	0.0493	0.997
	12	7.46	0.0653	0.996
HNR	4	17.83	0.0986	0.994
	12	15.01	0.0654	0.998

Text S4 Quantitative phase analysis of the mixtures of hematite and goethite using the intensity of characteristic peaks.

According to the method developed by Liu et al. (1994) ¹⁰, the quantitative phase analysis of the transformation products of hematite in the presence of Fe³⁺ and Al³⁺ were calculated by the intensities of characteristic peaks of hematite and goethite according to the following equation (eq.6):

$$\text{Goethite percentage} = \text{IntGoe}(110) / (3.5 \times \text{IntHem}(012) + \text{IntGoe}(110)) \quad (6)$$

where: IntGoe(110) and IntHem(012) are the diffraction peak intensities of goethite (110) plane and hematite (012) plane respectively. The calculated results are listed in **Table S3**.

Table S3 Proportions of goethite and hematite in the transformation products of hematite in the presence of Fe³⁺ and Al³⁺.

Sample	IntGoe(110)	IntHem(012)	Goe(□)	Hem(□)
HNP _{3d}	3829	4219	20.59	79.41
HNP _{7d}	2788	3323	19.34	80.66
HNC _{3d}	4589	3628	26.55	73.45
HNC _{7d}	5814	4739	25.95	74.05
HNR _{3d}	4991	5966	19.29	80.71
HNR _{7d}	3721	4905	17.81	82.19

Text S5. Mineral transformation Control experiment.

0.3 g of synthetic hematite crystals and 1.5 mM Al^{3+} were mixed in 200 mL of nitrogen-purged ultrapure water at 90 °C, followed by the addition of 120 mL 1 M KOH solution and 20 mL 1 M NaHCO_3 solution preheated at 90 °C. Then the reaction was conducted at 90 °C. At 7 d, 20 mL suspensions were withdrawn and centrifugated. The obtained solid was then washed, dried and ground. The transformation products were characterized by powder XRD.

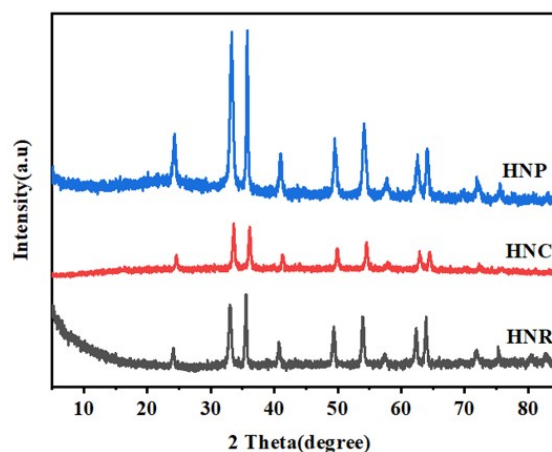


Figure S7. Powder XRD patterns of the transformation products of hematite crystals exposed different faces in the presence of Al^{3+} after reaction for 7 days at 90 °C.

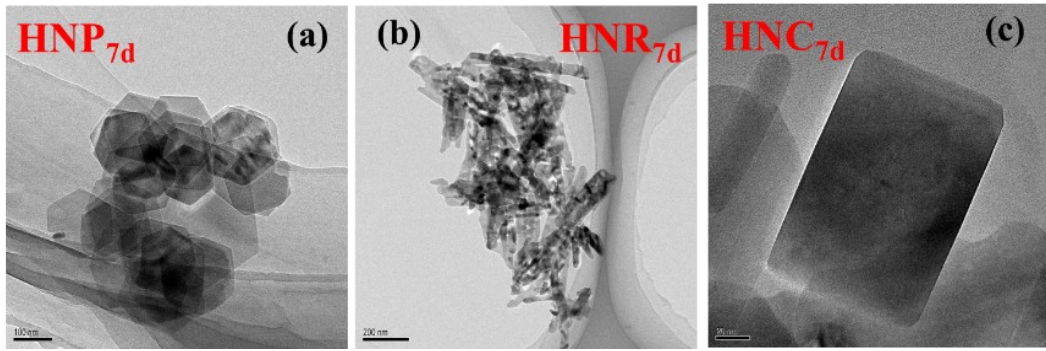


Figure S8. SAED patterns of the original morphology of the three kinds of synthetic hematite crystals in the presence of Fe^{3+} and Al^{3+} after reaction for 7 d. (a) $\text{HNP}_{7\text{d}}$, (b) $\text{HNR}_{7\text{d}}$ and (c) $\text{HNC}_{7\text{d}}$.

Table S4 EDS analysis of the transformed products from the three kinds of hematite samples in the presence of Fe³⁺ and Al³⁺.

Sample	HNP _{3d}		HNP _{7d}	
	Hem(HNP)	Goe	Hem(HNP)	Goe
Al content (mol.%)	0.94	1.52	0.88	1.84
	0.77	1.54	0.87	1.76
	0.83	1.62	0.9	1.58
	0.86	1.66	0.85	1.29
	0.84	1.64	0.84	1.46
	0.76	0.97	0.92	1.52
Average	0.83 ± 0.07	1.49 ± 0.26	0.88 ± 0.03	1.58 ± 0.20
Sample	HNC _{3d}		HNC _{7d}	
	Hem(HNC)	Goe	Hem(HNC)	Goe
Al content (mol.%)	0.96	1.52	1.14	1.54
	0.94	1.48	1.23	0.86
	0.92	1.36	1.16	1.25
	0.98	1.01	1.24	1.56
	1.12	1.03	1.31	1.02
	1.01	0.86	1.08	1.42
Average	0.99 ± 0.07	1.21 ± 0.28	1.19 ± 0.08	1.28 ± 0.29
Sample	HNR _{3d}		HNR _{7d}	
	Hem(HNR)	Goe	Hem(HNR)	Goe
Al content (mol.%)	2.18	1.46	3.14	1.86
	2.43	1.52	3.88	1.92
	2.15	1.45	4.12	2.06
	2.31	1.62	3.96	1.54
	1.76	1.31	3.15	1.04
	1.95	1.42	3.2	1.32
Average	2.13 ± 0.24	1.46 ± 0.10	3.58 ± 0.46	1.62 ± 0.39

Reference

1. V. Barrón and J. Torrent, Surface Hydroxyl Configuration of Various Crystal Faces of Hematite and Goethite, *J. Colloid Interface Sci.*, 1996, **177**, 407-410.
2. J. Lv, Y. Miao, Z. Huang, R. Han and S. Zhang, Facet-Mediated Adsorption and Molecular Fractionation of Humic Substances on Hematite Surface, *Environ. Sci. Technol.*, 2018, **52**, 11660-11669.
3. Y. Liang, J. Xu, L. K. Koopal, M. Wang and W. Tan, Facet-dependent surface charge and Pb²⁺ adsorption characteristics of hematite nanoparticles: CD-MUSIC-eSGC modeling, *Environ. Res.*, 2020, **196**, 110383.
4. T. Li, W. Zhong, C. Jing, X. Li and W. Chen, Enhanced Hydrolysis of p-Nitrophenyl Phosphate by Iron (Hydr)oxide Nanoparticles: Roles of Exposed Facets, *Environ. Sci. Technol.*, 2020, **54**, 8658-8667.
5. B. A. Legg, M. Baer, J. Chun, G. K. Schenter and J. Yoreo, Visualization of Aluminum Ions at the Mica Water Interface Links Hydrolysis State-to-Surface Potential and Particle Adhesion, *J. Am. Chem. Soc.*, 2020, **143**, 6093-6102.
6. L.C.Lan, L. W. Sheng, and M.Y. Zhu, DFT Studies on the Al-Speciation and Its Structure in Aqueous Aluminum Sol Formed by Aluminum Formoacetate, *J. Phys. Chem. B*, 2019, **123**, 9167-9179.
7. C. R. Frink and M. Peech, Hydrolysis of the Aluminum Ion in Dilute Aqueous Solutions, *Inorg. Chem.*, 1963, **2**, 473-478.
8. T. Z. Hao, X.Q. Peng, C.Yang, C.L.Guan, J.H.Yong, Study on the surface crystallization mechanism and inhibition method in the CMP process of aluminum alloy mirrors, *Appl. Opt.*, 2019, **58**, 6091-6097.
9. J. Berkowitz, M. A. Anderson and R. C. Graham, Laboratory investigation of aluminum solubility and solid-phase properties following alum treatment of lake waters, *Water Res.*, 2005, **39**, 3918-3928.
10. F. Liu, F. Xu, X. Li, Y. Wang and G. Zang, Types of Crystalline Iron Oxides and Phosphate Ad-sorption in Variable Charge Soils, *Pedosphere*, 1994, **01**, 35-46.